Physical Properties of Surfactant Bilayer Membranes: Thermal Transitions, Elasticity, Rigidity, Cohesion, and Colloidal Interactions

ARTICLE *in* THE JOURNAL OF PHYSICAL CHEMISTRY · JULY 1987

Impact Factor: 2.78 · DOI: 10.1021/j100300a003

2 AUTHORS:

Evan Evans
Boston University
24 PUBLICATIONS **2,311** CITATIONS
SEE PROFILE

David Needham
Duke University
12 PUBLICATIONS **1,093** CITATIONS
SEE PROFILE

Physical properties of surfactant bilayer membranes: thermal transitions, elasticity, rigidity, cohesion and colloidal interactions

Evan. Evans, and David. Needham

J. Phys. Chem., **1987**, 91 (16), 4219-4228• DOI: 10.1021/j100300a003 • Publication Date (Web): 01 May 2002

FEATURE ARTICLE

Physical Properties of Surfactant Bilayer Membranes: Thermal Transitions, Elasticity, Rigidity, Cohesion, and Colloidal Interactions

Evan Evans*

Pathology and Physics, University of British Columbia, Vancouver, B.C., Canada V6T 1W5

and David Needham

Mechanical Engineering and Material Science, Duke University, Durham, North Carolina 27706
(Received: February 2, 1987)

Simple micromechanical methods provide direct measurements of surface cohesion, elasticity, rigidity, and mutual attraction properties of surfactant double-layer membranes in aqueous media. Temperature-dependent tests yield explicit data for thermal phase transitions. Properties of mixtures of phospholipids (neutral and charged), cholesterol, and polypeptides have been studied. The results are essential for evaluation of theories of surfactant mixing, lamellar phase transitions, colloidal stabilization, and flocculation.

Introduction

The lamellar configuration of biological membrane structures is peculiar to the preferential assembly of amphiphilic molecules into molecular double layers. The strong preference for the lamellar configuration is evidenced by the negligible solubility of these molecules—and extremely slow rate of exchange from a membrane capsule—in aqueous media. In this condensed state, bilayer membranes exhibit solid- or liquidlike material behavior with the common feature of limited surface compressibility (i.e. great resistance to change in surface density). Because of the thin structure ($\sim$(3–4) $\times$ 10^{-7} cm), bilayer fragility and limited detectability by optical methods create significant obstacles to measurement of the physical-mechanical properties. Recently, micromechanical techniques have been developed to investigate thermal transitions, cohesion, elasticity, and surface rigidity of bilayer membranes in situ.[1-3]

Bilayers interact nonspecifically via long-range electrostatic, electrodynamic, and solvation forces.[4-8] These colloidal forces are commonly recognized as van der Waals attraction, electric double-layer repulsion, and hydration repulsion. Other steric and structural interactions exist that are not yet clearly understood. Even though the magnitude of each interaction can be very large, the free energy minimum at stable contact is extremely low. Again because of micromechanical technology, it is possible to directly measure the cumulated free energy potential for assembly (adhesion) of membrane surfaces to stable contact.[3,9-12]

In this article, we discuss how mixtures of lipids, cholesterol, and polypeptides affect the thermal-mechanical and colloidal interaction properties of bilayer membranes. We outline prominent physical features of bilayer membrane materials as solid and liquid surface structures. We examine how amphiphilic mixtures influence membrane cohesion and colloidal attraction. Finally, we evaluate the efficacy of classical prescriptions for van der Waals attraction and electric double-layer repulsion to correlate measured free energy potentials for adhesion. Lipids from two classes are discussed: phospholipids (phosphatidylcholine (PC), phosphatidylethanolamine (PE), phosphatidylserine (PS), and phosphatidylglycerol (PG)) and a "sugar" lipid (digalactosyl diacyl glycerol (DGDG)). The former are ubiquitous constituents of animal cell membranes whereas the latter exists predominantly in plant cell membranes.

Membrane Deformation, Mechanics, and Constitutive Relations[13,14,20]

For thin materials, deformation and rate of deformation are quantitated by variables that represent a sequence of simple shape changes for local regions (elements) of the surface: area dilation or condensation, $\alpha = \Delta A/A_0$; in-plane extension, $\bar{\lambda} = L/L_0$ (i.e. surface shear), at constant surface density; and bending or curvature change, $\Delta C = \Delta(1/R)$, without change in rectangular shape. These independent deformations are illustrated in Figure 1. External forces applied to a membrane are distributed throughout the surface as forces and moments per unit length along membrane contours (specific actions are shown in Figure 1), e.g. tension, τ_n, normal to the contour and surface (in-plane) shear, τ_s, tangent to the contour, transverse shear, Q_s, normal to the surface, and moment resultants (membrane "couples"), M. Pressures applied normal to the membrane are balanced primarily by tension components multiplied by appropriate curvatures. Shear stresses tangent to the membrane are opposed primarily by the surface gradients of tension. Membrane bending moments and transverse shear provide higher order contributions to these force balances.

There are three first-order elastic (conservative) relations for a surface-isotropic material: (1) mean tension, $\bar{\tau}$, proportional to the fractional area dilation or condensation

$$\bar{\tau} = K\alpha; \quad \bar{\tau} \equiv (\tau_1 + \tau_2)/2$$

(1) Kwok, R.; Evans, E. *Biophys. J.* **1981**, *35*, 637.
(2) Evans, E.; Kwok, R. *Biochemistry* **1982**, *21*, 4874.
(3) Evans, E.; Needham, D. *Faraday Discuss. Chem. Soc.*, in-press.
(4) Verwey, E. J. W.; Overbeek, J. Th. G. *Theory of the Stability of Lyophobic Colloids*; Elsevier: Amsterdam, 1948.
(5) Parsegian, V. A.; Fuller, N.; Rand, R. P. *Proc. Natl. Acad. Sci. U.S.A.* **1979**, *76*, 2750.
(6) Parsegian, V. A. *Annu. Rev. Biophys. Bioeng.* **1973**, *2*, 221.
(7) Israelachvili, J. N.; Pashley, R. M. In *Biophysics of Water*, Franks, F., Ed.; Wiley: New York, 1982; p 183.
(8) Rand, R. P. *Annu. Rev. Biophys. Bioeng.* **1981**, *10*, 277.
(9) Evans, E.; Metcalfe, M. *Biophys. J.* **1984**, *45*, 715.
(10) Evans, E.; Metcalfe, M. *Biophys. J.* **1984**, *46*, 423.
(11) Marra, J.; Israelachvili, J. *Biochemistry* **1985**, *24*, 4608.
(12) Marra, J. *J. Colloid Interface Sci.* **1985**, *107*, 446.
(13) Evans, E.; Skalak, R. *Mechanics and Thermodynamics of Biomembranes*; CRC: Boca Raton, FL, 1980.
(14) Evans, E. In *NATO Advanced Study Institute Textbook on Biorheology*, Hwang and Gross, Eds.; Sitjhoff and Noordhoff: 1981; p 137.

0022-3654/87/2091-4219$01.50/0

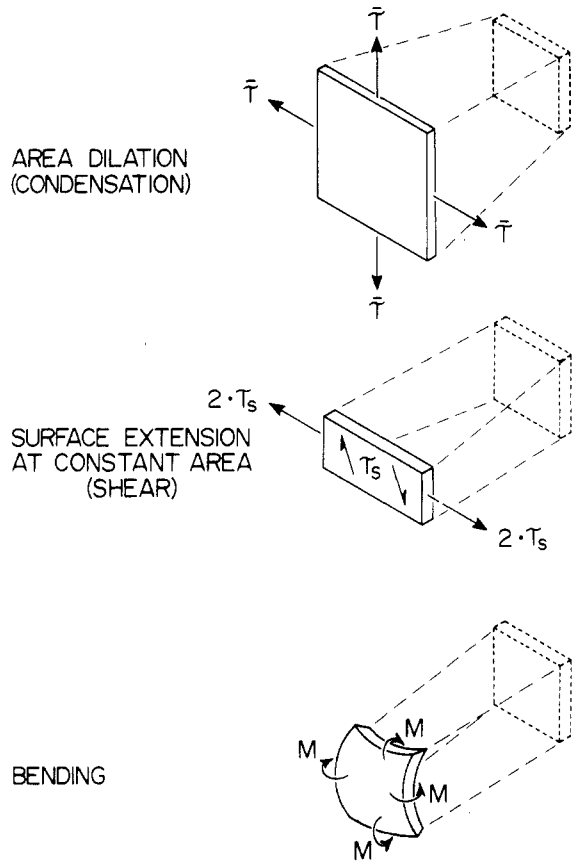

Figure 1. Independent modes of deformation and force-moment resultants for an element of a thin-surface material.

where τ_1 and τ_2 are principal values of tension for orthogonal directions tangent to the surface; (2) surface shear, τ_s, proportional to in-plane extension or shear strain:

$$\tau_s = \mu(\tilde{\lambda}^2 - \tilde{\lambda}^{-2})/2 = 2\mu e_s; \quad \tau_s \equiv (\tau_1 - \tau_2)/2$$

(3) bending moments M proportional to changes in membrane curvatures

$$M = B\Delta(1/R_1 + 1/R_2)$$

The *first* elastic relation represents the compressibility of the surface at constant temperature and does not distinguish between solid and liquid structures except by relative value. Coupled with separate measurement of thermal area expansivity (fractional change in area with temperature, $\partial\alpha/\partial T$), the surface compressibility modulus, K, yields the heat of expansion per unit surface area at constant temperature[15]

$$\frac{1}{A}\left(\frac{\partial Q}{\partial \alpha}\right)_T = TK\left(\frac{\partial \alpha}{\partial T}\right)$$

which is related to the lateral pressure within the bilayer. The *second* elastic relation is unique to solid structures; liquids are defined by the state of zero shear modulus ($\mu \equiv 0$). Thus, shear rigidity is peculiar to frozen (crystalline) bilayers. Because of crystal defects in the frozen bilayer, deformation of a frozen vesicle exhibits a limited elastic response followed by yield and surface flow. Flow commences at very small shear strains and only the surface rigidity, $\hat{\tau}_s$, at yield is readily measured for the frozen bilayer. The *third* elastic relation represents the curvature elasticity of the bilayer. Due to the extreme thinness of the bilayer, bending rigidity offers little opposition to deformation for bilayer capsules which are cell size in dimension.[1,13] However, if there is a superlattice (ripple) corrugation of the bilayer, the small bending rigidity leads to a special extensional stiffness.[16]

(15) Evans, E.; Waugh, R. E. *J. Colloid Interface Sci.* **1977**, *60*, 286.
(16) Evans, E. In "Festkorperprobleme" In *Advances in Solid State Physics*, Vol. 25, Grosse, P., Ed.; Vieweg: Braunschweig, 1985; p 735.

Similar to ideal elastic relations, viscous-liquid (nonconservative) responses of a bilayer are proportionalities between force-moment resultants and *rates* of deformation, i.e.

$$\bar{\tau} = \kappa\frac{\partial \ln (1 + \alpha)}{\partial t}$$

$$\tau_s = 2\eta\frac{\partial \ln (\tilde{\lambda})}{\partial t}$$

$$M = \nu\frac{\partial(\Delta C)}{\partial t}$$

The coefficients are surface viscosities (κ,η,ν) for dilation, shear, and bending, respectively. When the acyl chains are liquid, viscous dissipation in the bilayer is difficult to measure because the deformation response of cell-size capsules is dominated by dissipation in the adjacent aqueous phases.[20] Viscosities for area dilation and curvature changes appear to be completely inaccessible to mechanical measurement because they are determined by relaxation times for acyl chain extension ($\lesssim 10^{-7}$ s).[21] Since these deformations are usually elastic, viscosities for dilation and bending deformations may be estimated from the elastic moduli multiplied by the relaxation time, t_e, for chain extension

$$\kappa \sim Kt_e$$

$$\nu \sim Bt_e$$

Surface diffusivity measurements of fluorescent membrane probes can be used to estimate the surface shear viscosity of lipids in the liquid state; the results are on the order of 10^{-6}–10^{-5} dyn s/cm.[17-20] On the other hand, dynamic deformations of cell-size vesicles provide extremely useful methods for study of bilayer yield and flow in the frozen (solid) state. Here, the shear viscosity is so large that measurements of probe diffusivity become unreliable. Mechanical transition of the bilayer from solid to liquid behavior is modeled by an ideal plastic relation, i.e. solid below a yield threshold and perfect liquid above the yield

$$\tau_s - \hat{\tau}_s = 2\eta\frac{\partial \ln (\tilde{\lambda})}{\partial t}; \quad \tau_s \geq \hat{\tau}_s$$

Vesicle Deformation Tests and Methods of Analysis

Diacyl lipids spontaneously form closed vesicular capsules when hydrated from an anhydrous state. Although small in number, a few of these capsules are of sufficient size ((10–20) × 10^{-4} cm) that they can be subjected to direct micromechanical deformation and adhesion tests. Production of big vesicles is most likely when lipids are hydrated by either water or aqueous solutions of nonelectrolytes (e.g. sugars) above the acyl chain crystallization temperature.[22-23] Nonelectrolytes also enhance optical images when vesicles are resuspended in salt solution and viewed with interference contrast optics (Figure 2 shows vesicle images with/without refractile solutes). Single vesicles are selected from one chamber on a microscope stage and transferred into a solution (usually a buffered 0.1 M NaCl solution) which is made slightly more concentrated than the nonelectrolyte solution used for lipid hydration. Partial deflation of the vesicle follows which allows large projections to be aspirated into the selection pipet.

Vesicle deformation tests are based on simple pressurization by micropipet suction. After the vesicle is pressurized into a spherical shape, further suction acts to dilate the surface area and reduce internal volume. Because the pressures involved in these tests are several orders of magnitude smaller than the pressure required to filter water from the vesicle (against osmotic activity

(17) Derzko, Z.; Jacobson, K. *Biochemistry* **1980**, *19*, 6050.
(18) Saffman, P. G.; Delbruck, M. *Proc. Natl. Acad. Sci. U.S.A.* **1975**, *72*, 3111.
(19) Galla, H. J.; Hartmann, W.; Theilen, U.; Sackmann, E. *J. Membr. Biol.* **1979**, *48*, 215.
(20) Evans, E.; Hochmuth, R. M. In *Current Topics in Membranes and Transport*, Vol. 10, Bronner, F., Kleinzeller, A., Eds.; Academic: New York, 1978; p 1.
(21) Bloom, M.; Smith, I. C. P. In *Progress in Protein-Lipid Interactions*, Watts, De Pont, Eds.; Elsevier: New York, 1985; p 61.
(22) Reeves, J. P.; Dowben, R. M. *J. Cell. Biol.* **1969**, *73*, 49.
(23) Needham, D.; Evans, E. *Biochemistry*, to be submitted.

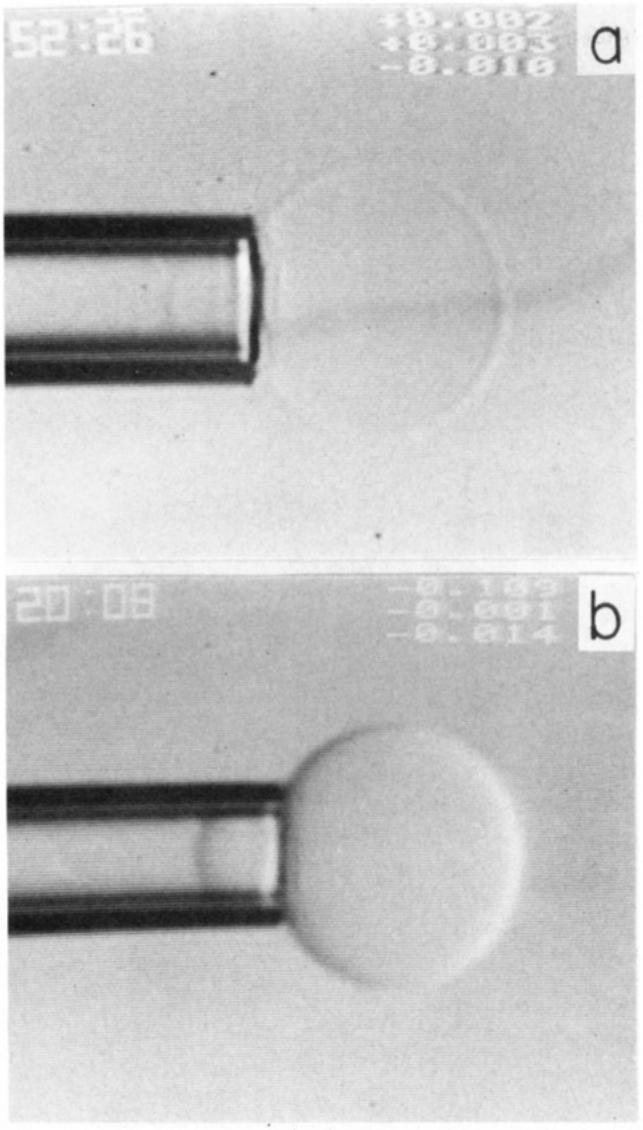

Figure 2. Video micrographs of giant bilayer vesicle aspiration (vesicle diameter $\sim 20 \times 10^{-4}$ cm; pipet diameter $\sim 6 \times 10^{-4}$ cm). (a) Vesicle without refractile solutes in distilled water. (b) Vesicle with 0.1 M sucrose inside and 0.1 M NaCl outside.

of the trapped solutes), vesicle volumes remain constant. Small changes in projection length, L, are proportional to the change in total area, A, of the vesicle scaled by pipet and vesicle dimensions (R_P, R_0)[1]

$$\Delta A \cong 2\pi R_p(1 - R_p/R_0)\,\Delta L$$

Area changes are greatly amplified which facilitates detection of the small elastic compressibility ($\Delta A/A_0 \sim 10^{-2}$) of the surface. The mean tension, $\bar{\tau}$, is uniform over the entire vesicle surface and is given by the suction pressure, P, and pipet/vesicle dimensions[1]

$$\bar{\tau} = PR_p/(2 - 2R_p/R_0)$$

The slope of the tension vs. area dilation is the elastic area compressibility modulus, K. With selection first of the thinnest vesicles as imaged by interference contrast and then evaluation of the area elastic modulus, it is possible to discriminate between one, two, and more layers since the elastic modulus groups around discrete values where the lowest value is characteristic of a single bilayer.[1]

Another feature of vesicle pressurization is that thermal transitions in the surface density can be observed at a controlled state of stress.[2] Large initial projections of the vesicle into the pipet enable measurement of large condensations in surface density ($\sim$20%) without retraction from the pipet. Note, changes in length inside the pipet represent changes in the "projected" area of the bilayer. When submicroscopic structures like ripples are present, both changes in density of the molecules as well as ripple architecture contribute to the displacement of the length.[23]

Deflation of spherical vesicles produces flaccid irregular shapes which are effectively stress free.[68] Initial aspiration takes only very small pressures ($\sim 10^{-6}$ atm) when the bilayer is in the liquid state and somewhat higher pressures ($\sim 10^{-4}$ atm) when the bilayer is frozen. These pressures are much smaller than the pressures ($\sim 10^{-2}$ atm) subsequently required to expand the surface area of sphered vesicles. This aspiration behavior reflects the hierarchy of bilayer rigidity properties: resistance to area dilation $\gg$ resistance to shear and bending. For a liquid bilayer surface, only bending rigidity resists initial deformation of the flaccid vesicle as it enters the tube. The threshold pressure for entry is given approximately by

$$P_0 \sim 8B/R_p^3$$

On the basis of the suction required for initial aspiration of a flaccid vesicle and pipet diameter ($\sim 5 \times 10^{-4}$ cm), the curvature elastic modulus, B, is estimated to be on the order of 10^{-12} dyn cm (erg), consistent with values derived from analysis of thermal fluctuations of vesicle contours and theoretical predictions.[24-26]

When the acyl chains are crystallized, initial aspiration pressures for partially deflated vesicles are dominated by the shear rigidity of the surface.[27] Below a threshold pressure, the vesicle is only slightly deformed by pipet suction and remains fixed in shape. Above this pressure, the vesicle deforms continuously and flows slowly into the tube until it reaches the pressurized spherical geometry where area dilation is required for further entry. Analysis shows that the threshold is proportional to the surface shear rigidity, $\hat{\tau}_s$.[27]

$$P_0 \sim 8\hat{\tau}_s \ln (R_0/R_p)/R_p$$

For constant suction in excess of the threshold pressure, the *rate* of entry $\dot{L}$ of the solid-bilayer vesicle is limited by the surface shear viscosity

$$\dot{L} \sim \Delta P R_p^2/[4\eta \ln (R_0/R_p)]; \quad \Delta P \equiv (P - P_0)$$

Transitions, Compressibility, Rigidity, and Cohesion of Single-Component Bilayers

Lamellar phases of lipids are either anisotropic liquids with fluid acyl chains or solids with crystallized chains.[28,29] The liquid phase is labeled L_α whereas the solid phase has several descriptors related to chain tilt and surface topography, e.g. planar crystalline phases (L_β, $L_{\beta'}$) and "rippled" or corrugated intermediate solid phases ($P_{\beta'}$). The prime superscript identifies layers where acyl chains are tilted with respect to the normal to the bilayer surface. The "main" enthalpic transition, T_c, separates liquid from solid phases whereas the "pre-" transition, T_p, correlates with the separate existence of planar-solid (below T_p) and rippled-solid (above T_p) surfaces. Lower "sub-" transitions have been identified and are currently under investigation.[30,31]

Saturated chain PC's exhibit $L_{\beta'}$, $P_{\beta'}$, and L_α phases. For example, dimyristoylphosphatidylcholine (DMPC) below 10–13 °C is a $L_{\beta'}$ solid at equilibrium, a $P_{\beta'}$ solid above 13 °C but below 24 °C, and a L_α liquid surface above 24 °C.[32] Figure 3 shows

(24) Servuss, R. M.; Harbich, W.; Helfrich, W. *Biochim. Biophys. Acta* **1978**, *436*, 900.
(25) Engelhardt, H.; Durve, H. P.; Sackmann, E. *J. Phys. Lett.* (*Paris*) **1985**, *46*, L395.
(26) Schneider, M. B.; Jenkins, J. T.; Webb, W. W. *J. Phys.* (*Paris*) **1984**, *5*, 1457.
(27) Evans, E.; Needham, D. *J. Colloid Interface Sci.*, to be submitted for publication.
(28) Luzzati, V. In *Biological Membranes*, Chapman, D., Ed.; Academic: New York, 1968; p 71.
(29) Luzzati, V.; Tardieu, A. *Annu. Rev. Phys. Chem.* **1974**, *25*, 79.
(30) Chen, S. C.; Sturtevant, J. M.; Gaffney, B. J. *Proc. Natl. Acad. Sci. U.S.A.* **1980**, *77*, 5060.
(31) Ruocco, M. J.; Shipley, G. G. *Biochim. Biophys. Acta* **1982**, *691*, 309.

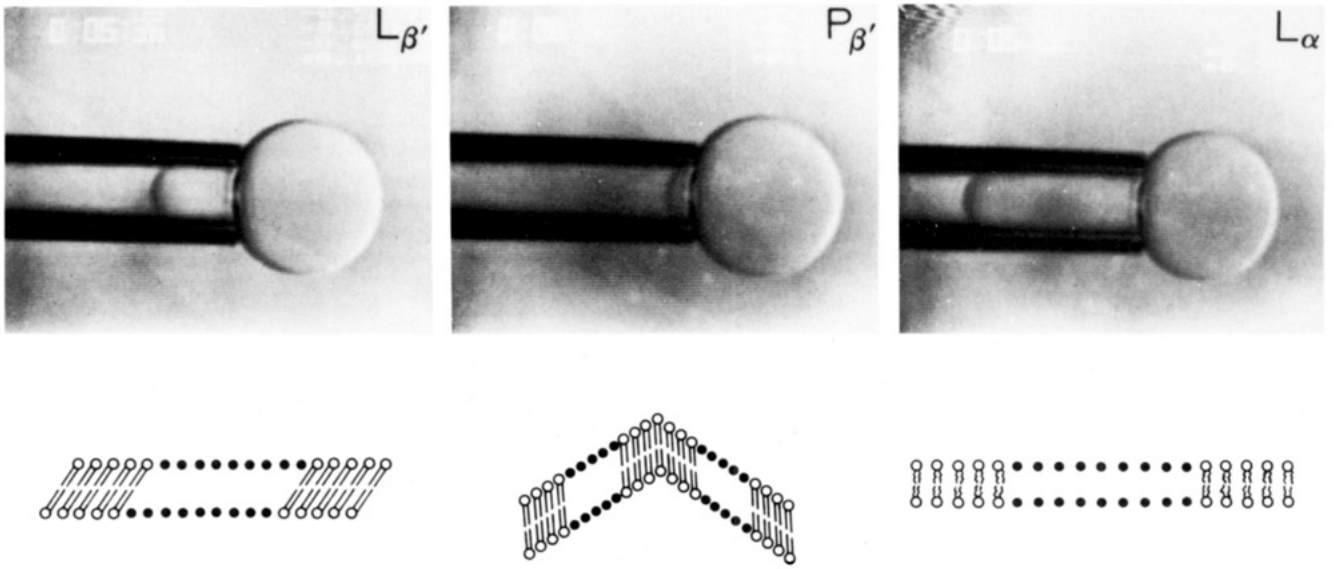

Figure 3. Video micrographs of a DMPC bilayer vesicle in three structural phases: left is $L_{\beta'}$ state at 8 °C; middle is $P_{\beta'}$ state at 16 °C; right is L_α state at 25 °C. Note: length in pipet represents *projected* area of bilayer structure.

an individual single-walled vesicle at specific temperatures characteristic of these phases. The intermediate $P_{\beta'}$ structure (ripple) can be eliminated or prevented from formation by moderate bilayer stress.[23] Also when vesicles are annealed at low temperatures (<10 °C) for a few days to ensure formation of $L_{\beta'}$ structure and then heated to temperatures above T_p in a short time period, the $P_{\beta'}$ ripple does not appear to form. Hence, metastable (planar) phases can exist between T_p and T_c, labeled as $L_{\beta'}^*$.[23] These observations are accumulated into a phase diagram (Figure 4) which demonstrates the importance of stress history in formation of the solid-phase structure.

The ratio of areas between the rippled state and the metastable planar state at the same temperature provides a direct measure of the intrinsic tilt of the chains relative to the surface (angles are listed in Figure 4). This conclusion is based on X-ray diffraction studies which show that the acyl chains are aligned nearly normal to the projected plane of the ripple in the $P_{\beta'}$ phase but are tilted to the flat surface in the $L_{\beta'}$ phase.[33] The results correlate very well with values derived from structural analysis by X-ray diffraction.[32] In addition, the fractional reduction in area from the L_α phase to the $P_{\beta'}$ phase at the main transition is a direct measure of the condensation of the acyl chains (~20%) upon freezing.

In the domain of the $P_{\beta'}$ phase, the tension vs. projected area exhibits an initial soft-elastic response at low tensions, then plastic (permanent) expansion at moderate tensions as the surface ripple is eliminated, and finally a stiff elastic response at the expanded area due to limited compressibility of the planar surface.[23] The initial soft-elastic response is consistent with extension of the surface corrugation due to bending deflections of individual pleats. The soft-elastic modulus is proportional to the bending modulus divided by the square of the peak-to-peak amplitude "a" of the surface ripple

$$K_{\text{apparent}} \sim 8B/a^2$$

Measurements for the initial elastic behavior (50–60 dyn/cm)[23] plus values of ripple amplitude from X-ray diffraction and SEM studies ((5–8) × 10^{-7} cm)[33,34] indicate that the bending stiffness is about 3 × 10^{-12} dyn cm at these temperatures.

After the $P_{\beta'}$ corrugation is removed by stress, it is possible to measure the surface compressibility of the planar bilayer. The area compressibility modulus increases only by about a factor of 2 from 1.2 × 10^2 to 2.8 × 10^2 dyn/cm when the surface is initially frozen from the L_α phase to the $P_{\beta'}$ domain. Below the pretransition temperature, the compressibility is greatly reduced (K ~ 10^3 dyn/cm). These results corroborate spectroscopic observations that indicate a large number of residual gauche chain conformations exist in the intermediate range of temperatures ($T_p < T < T_c$).[35-37] Hence, surface compressibility is sensitive to chain packing "defects" in the surface.

Partially unsaturated phospholipids (e.g. 1-stearoyl-2-oleoylphosphatidylcholine (SOPC) and 1-palmitoyl-2-oleoylphosphatidylethanolamine (POPE)) exhibit direct condensation from the L_α phase to the L_β phase without chain tilt or superlattice formation.[38,39] The area change upon freezing is about 20%

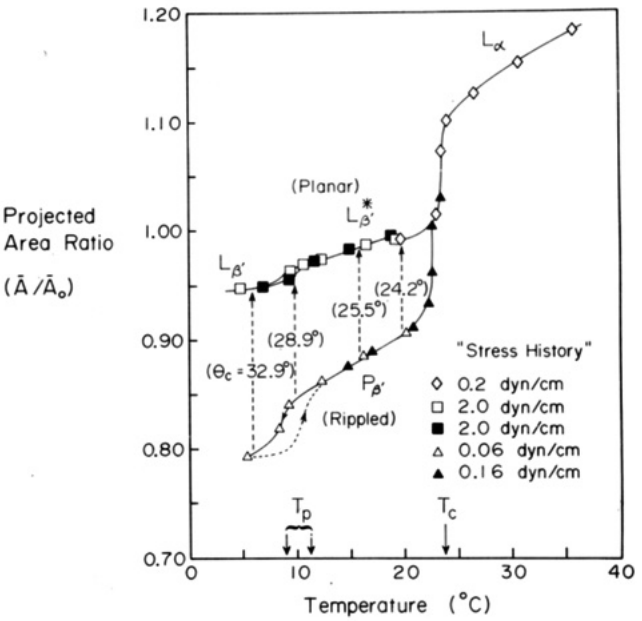

Figure 4. Effect of bilayer stress on solid DMPC bilayer structure and phase formation. Relative vesicle area is plotted vs. temperature for fixed bilayer tensions. Values of the acyl chain tilt to the bilayer normal (angles in parentheses) were derived from the ratio of projected areas for the rippled-solid and planar-solid surfaces at the same temperature.

(32) Janiak, M. J.; Small, D. M.; Shipley, G. G. *Biochemistry* **1976**, *21*, 4575.
(33) Stamatoff, J.; Fever, B.; Guggenheim, M. J.; Teller, G.; Yamane, T. *Biophys. J.* **1982**, *38*, 217.
(34) Krebecek, R.; Gebhardt, C.; Gruber, M.; Sackmann, E. *Biochim. Biophys. Acta* **1979**, *554*, 1.
(35) Brady, G. W.; Fein, D. B. *Biochim. Biophys. Acta* **1977**, *646*, 249.
(36) Davis, J. H. *Biophys. J.* **1979**, *27*, 339.
(37) Wong, P. T. *Annu. Rev. Biophys. Bioeng.* **1984**, *13*, 1.
(38) Davis, P. J.; Fleming, B. D.; Coolbear, K. P.; Keough, K. M. *Biochemistry* **1981**, *20*, 3633.

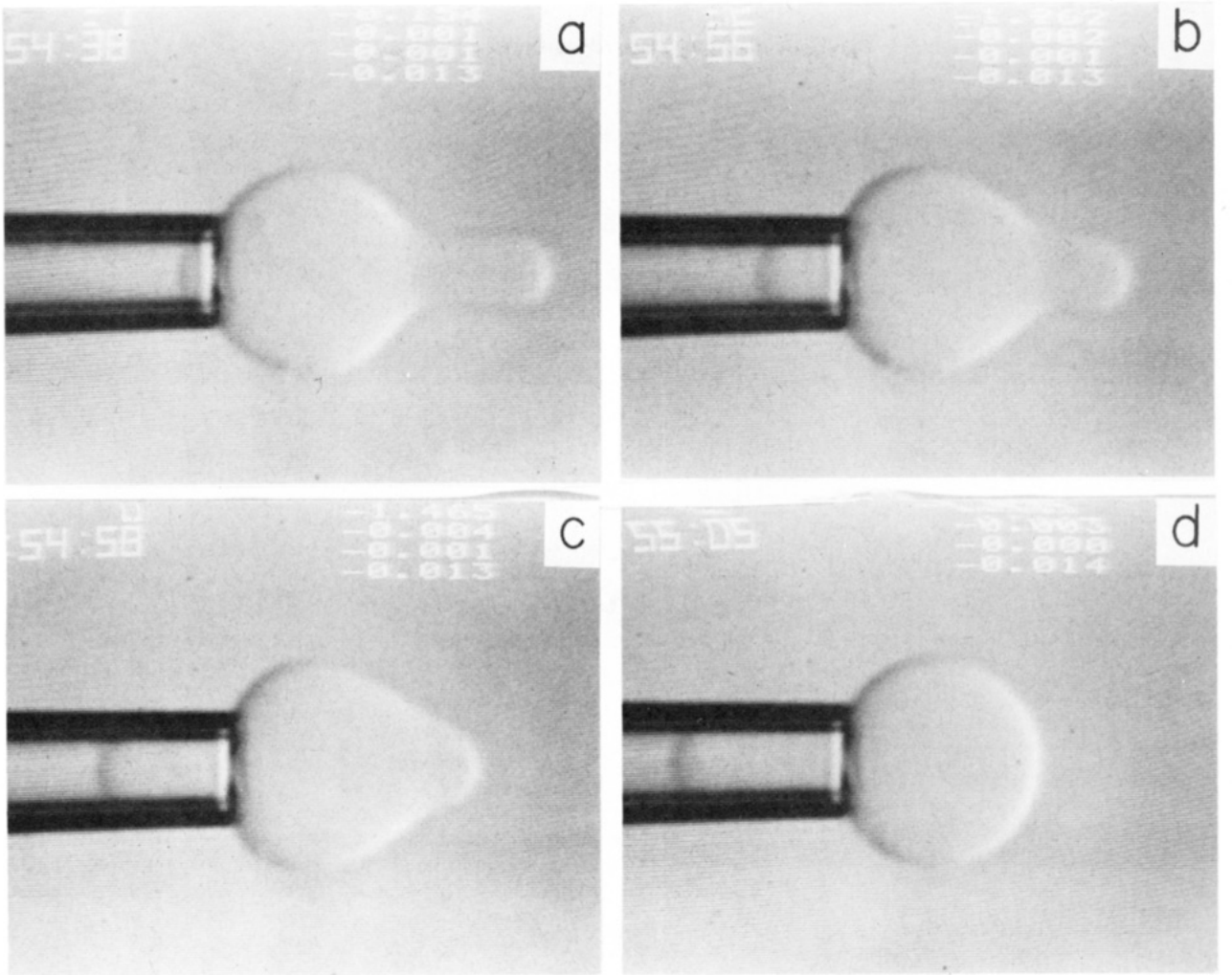

Figure 5. Video micrographs of a frozen DMPC vesicle (13 °C). (a) Vesicle as frozen replica of aspiration at high suction pressure, reversed for reaspiration. (b) Threshold suction sufficient to exceed surface shear rigidity (yield). (c) An image taken during continuous flow at elevated suction above yield threshold. (d) Final pressurization to a solid sphere.

similar to DMPC.[3] Area compressibility moduli in the L_α phase for these two lipids are comparable ($(2.0–2.3) \times 10^2$ dyn/cm) but higher than for DMPC. Values of compressibility moduli in the L_β phase are similar to that for DMPC in the $L_{\beta'}$ phase ($\sim 10^3$ dyn/cm). The sugar-lipid DGDG (a natural product with three double bonds) has an area compressibility modulus which is slightly lower (1.9×10^2 dyn/cm) than for SOPC or POPE. To compare moduli of surface compressibility with values characteristic of volumetric compressibility for solids (10^{12} dyn/cm^2), liquids (10^{10} dyn/cm^2), and gases (10^6 dyn/cm^2), surface moduli are divided by a representative value for the bilayer thickness (3×10^{-7} cm). We see that bilayers as condensed surface materials are 10–100 times more expandable than ordinary liquids!

Like compressibility, the thermal area expansivity of bilayers is much greater than the volumetric expansivity ($\sim 10^{-4}$/°C) of condensed liquids. In the L_α and $P_{\beta'}$ domains, the fractional change in vesicle area with temperature describes the chain expansivity with temperature. In the $L_{\beta'}$ domain, the change in vesicle area with temperature is related to the chain expansion and changes in chain tilt. There is little difference in thermal area expansitivity ($(5–6) \times 10^{-3}$/°C) for DMPC bilayers in the L_α and $P_{\beta'}$ phases. Thermal area expansivity is significantly lower in the $L_{\beta'}$ phase of DMPC but accurate values are difficult to obtain because of the limited range of accessible temperatures. Similarly, POPE and SOPC exhibit thermal area expansivities of about 3×10^{-3}/°C in the L_α phase and $(1–2) \times 10^{-3}$/°C in the frozen L_β phase. The thermal area expansivity for DGDG is also lower (2×10^{-3}/°C) than for the L_α phase PC's. Hence in the absence of density transitions, bilayers expand a few percent in area when the temperature is increased by 10 °C.

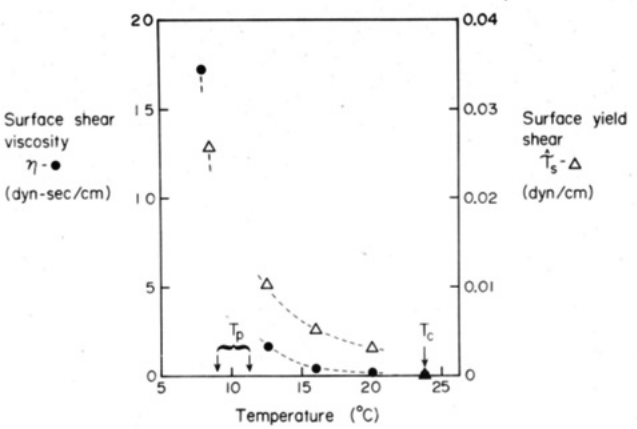

Figure 6. Surface shear viscosity (left ordinate) and surface shear rigidity (right ordinate) are plotted as a function of temperature derived from measurements on frozen DMPC vesicles below the main acyl chain transition (T_c) and pretransition (T_p).

Surface rigidity is peculiar to solid bilayer phases. Figure 5 shows a frozen DMPC vesicle first pulled tight into micropipet then ejected as a solid replica of the pipet cavity and reversed for reaspiration. Threshold pressures—and subsequent *rates* of vesicle entry into the pipet at higher pressures—are analyzed to determine the surface shear rigidity and viscosity.[27] Figure 6 shows abrupt augmentation in rigidity and viscosity for solid DMPC surfaces as the temperature is reduced below the pretransition T_p to the

(39) McIntosh, T. J. *Biophys. J.* **1980**, *29*, 237.

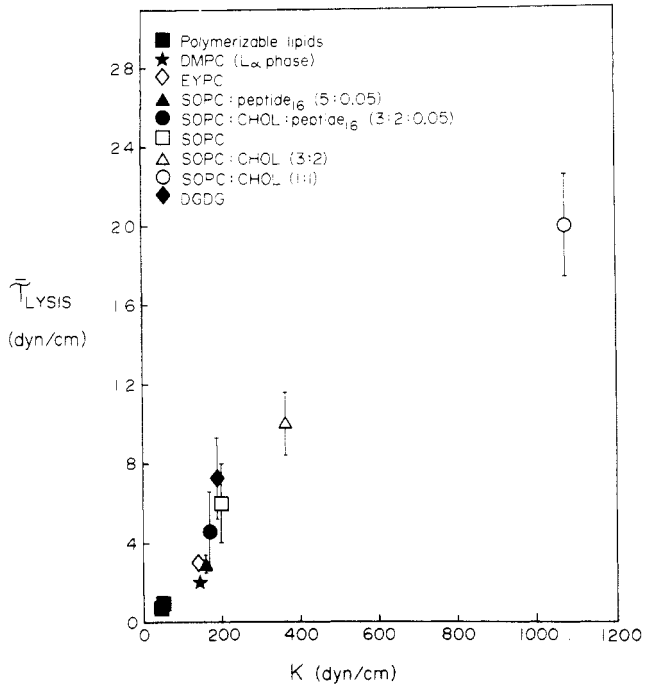

Figure 7. Values for bilayer tension at vesicle rupture vs. elastic area compressibility moduli for all lipid compositions studied to date.

highly condensed low temperature domain. Close to the main transition, the surface viscosity is four orders of magnitude larger than expected for the L_α phase based on measurement of lateral diffusivity of fluorescent probes.[20] Shear rigidity and viscosity primarily reflect the density and mobility of crystal defects in the surface.

Solid and liquid bilayers fail by area dilation which leads to vesicle rupture or lysis. Although lysis is expected to be a stochastic process that involves the time of exposure to the stress, experimental observations show precipitous failure when the tension reaches a critical value with reasonably long-term survival of vesicles below this tension. For DMPC vesicles, lysis occurs at 2–3 dyn/cm in the L_α phase but more than 15 dyn/cm is required in the $L_{\beta'}$ phase. SOPC, POPE, and DGDG are more resistant to lysis in the L_α phase than DMPC (i.e. about 6 dyn/cm tension for rupture); similarly, SOPC and POPE bilayers become significantly more resistant to lysis in the frozen state (Figure 7). This general feature has been seen in all of our vesicle studies, i.e. tension levels for lysis increase as the lipid area compressibility is reduced. Correlation of lysis tension with compressibility modulus indicates that critical fluctuations in surface density may be the origin of failure.

Thermochemical Properties of Bilayer Mixtures

Natural membranes are composites of lipids, integral and peripheral proteins, cholesterol, etc. The PC and PE classes of lipids, especially those with asymmetric chain composition and saturation, are major components of cell membranes. Mixtures of two of these lipids (SOPC and POPE) with similar chain length composition have been studied over a temperature range that spans both acyl chain crystallization transitions at pH 6.0 where both lipids are electrically neutral.[3] Based on onset and final temperatures for each mixture transition, a phase diagram can be constructed which correlates with no enthalpy of mixing and ideal entropy of mixing. Hence, the two lipids are essentially miscible in both liquid and solid phases except for PE contents below 33% where some of the SOPC appears to freeze separately.[3,40-42] Values for area compressibility moduli, measured at temperatures just above the main transition in the L_α phase of both components, show a slight linear compositional dependence (Table I) consistent with ideal mixing. Thermal area expansivities for the mixtures are similar to values for the single components in the L_α phase when well above the acyl chain crystallization temperature. Based on observation of the tensions required to lyse (rupture) vesicles, these neutral lipid mixtures exhibit bilayer cohesion levels similar to single-component membranes.

TABLE I: Thermoelastic Properties of SOPC:POPE Bilayers

POPE/ (SOPC + POPE)	K, dyn/cm	$\dot{\alpha}$, $\times 10^3$/°C	T, °C
0	199.6 ± 12.7	3.28 ± 0.68	15.0
0.33	209.9 ± 14.1	3.79 ± 0.24	22.0
0.60	221.4 ± 11.2	3.51 ± 0.57	25.0
0.80	233.7 ± 26.0	3.53 ± 0.49	26.0

TABLE II: Thermoelastic Properties of Lipid:Cholesterol Mixtures

composition	K, dyn/cm	$\dot{\alpha}$, $\times 10^3$/°C	T, °C
DMPC (L_α)	144.9 ± 10.5	6.81 ± 1.0	29
		4.17 ± 0.2	35
DMPC ($L_{\beta'}$)	855.3 ± 140.1	1.0	8
CHOL/(DMPC + CHOL)			
0.125	396.9	2.83	15.5
0.33	646.8	1.97	15
	559.0	3.1	25
0.40	600	2.3	35
0.50	685	1.33	22
SOPC (L_α)	199.6 ± 12.7	3.28 ± 0.68	15
CHOL/(SOPC + CHOL)			
0.5	1077 ± 167	1.62 ± 0.16	23

Mixtures of DMPC, SOPC, and cholesterol (CHOL) have been used to examine the effects of cholesterol on the chain crystallization transitions.[3,43] Vesicle area vs. temperature plots show that the main transition broadens and shifts to higher temperatures as the concentration of cholesterol is increased in agreement with regular solution theory.[43] Similar results have been obtained in scanning calorimetry and NMR studies.[44,45] Upon addition of cholesterol to DMPC (even small amounts), the $P_{\beta'}$ phase seems to disappear and a tilted geometry is indicated for isolated frozen lipid regions.[43] Area changes over the broadened transitions are reduced by cholesterol and disappear with addition of 50 mol % to leave the thermal area expansivity at 1.3×10^{-3}/°C. These area changes are consistent with separate formation of a 1:1 (DMPC:CHOL) complex that does not condense plus residual free lipid that condenses (freezes) normally.[43,46] Both above and below the broad transition, the elastic area compressibility modulus K is greatly increased with cholesterol addition (Table II). *However*, for all concentrations above 12.5 mol % (which exhibits only very weak surface rigidity), vesicle bilayers behave as surface liquids with no surface rigidity even at temperatures well below the solid-phase transition. Compared to bilayers in the liquid L_α state, introduction of cholesterol forms a tight complex with the lipid which greatly reduces bilayer compressibility (and permeability as evidenced by the extremely slow response of vesicles to osmotic dehydration) but maintains the bilayer in a liquid state well below the acyl chain crystallization temperature of the lipid. Addition of cholesterol to bilayers also greatly enhances bilayer cohesion (Figure 7).

In models of lipid–protein interaction, the mismatch between hydrophobic lengths of lipid chains and the transmembrane peptide sequence plays a major role in the solution-phase behavior.[47-49]

(40) Lewis, G. N.; Randall, M. *Thermodynamics*; McGraw Hill: New York, 1961.
(41) Shimshick, E. J.; McConnell, H. M. *Biochemistry* **1973**, *12*, 2351.
(42) Chapman, D.; Urbina, J.; Keough, K. M. *J. Biol. Chem.* **1974**, *249*, 2512.
(43) Needham, D.; McIntosh, T. J.; Evans, E. *Biochemistry*, to be submitted.
(44) Mabrey, S.; Mateo, P. L.; Sturtevant, J. M. *Biochemistry* **1978**, *17*, 2464.
(45) Vist, M. R.; Davis, J. H., to be submitted for publication.
(46) Presti, F. T.; Pace, R. J.; Chan, S. I. *Biochemistry* **1982**, *21*, 3831.
(47) Marcelja, S. *Biochim. Biophys. Acta* **1976**, *455*, 1.
(48) Owicki, J. C.; Springgate, M. W.; McConnell, H. M. *Proc. Natl. Acad. Sci. U.S.A.* **1978**, *75*, 1616.
(49) Mouritsen, O. G.; Bloom, M. *Biophys. J.* **1984**, *46*, 141.

TABLE III: Elastic Area Compressibility Modulus of Lipid, Lipid:Cholesterol, and Lipid:Cholesterol:Peptide Bilayer Mixtures

composition	K, dyn/cm	T, °C
SOPC (L_α)	199.6 ± 12.7	15
SOPC:CHOL (3:2)	362.7 ± 20.6	15
SOPC:peptide (5:0.05)	161.1 ± 23.6	15
SOPC:CHOL:peptide$_{16}$ (3:2:0.05)	168.9 ± 24.6	15
DMPC (L_α)	144.9 ± 10.5	29
DMPC:CHOL (3:2)	600	35
DMPC:CHOL:peptide$_{24}$ (3:2:0.05)	945 ± 218	12.5 ± 0.5
	245	29.5
	193 ± 31	34.4 ± 1.3

Preliminary experiments[3] on a simple lipid–peptide system have been carried out with two synthetic amphiphilic peptides: 16 and 24 hydrophobic leucine residues bounded by two lysines at the N and C terminals (long hydrophobic α-helices with hydrophilic ends). The effects of these peptides at low concentrations on area compressibility modulus of both lipid and lipid:cholesterol bilayers are listed in Table III. The introduction of peptide$_{16}$ into SOPC bilayers clearly increases the bilayer compressibility. Even though SOPC:CHOL (3:2) is much less compressible than pure lipid, the introduction of peptide produces an unexpectedly large increase in bilayer compressibility and reduced cohesion (Figure 7). Additional evidence that incorporation of the peptide alters the lipid–cholesterol interaction is obtained from measurements of area compressibility on DMPC:CHOL:peptide$_{24}$ mixtures. At high temperatures, the lipid–cholesterol–protein vesicles commence a broad but significant area transition (not present for the lipid–cholesterol mixture); here, the area compressibility is much greater with the peptide present than for the lipid–cholesterol mixture (Table III). At low temperatures, there is a striking reduction in area compressibility where the modulus increases to values even greater than for the lipid–cholesterol mixture. In the low-temperature region, cholesterol appears to form a close cohesive complex with the lipid whereas, at high temperatures, cholesterol appears to associate with the peptide to form islands in the compressible liquid phase of the lipid.

Colloidal Interactions between Bilayers

Separated by a medium with different polarizability properties, bilayers are drawn together by long-range van der Waals forces described by Lifshitz theory for continuous media.[50] Electrically charged lipids in salt solutions oppose this attraction with double-layer forces at large distances; but at short distances, solvation and structure forces associated with the intervening liquid and surfactant head groups dominate repulsion for all lipids.[4-8] Reversible adhesion will occur if the attraction is sufficient to overcome long-range repulsion but not sufficient to overwhelm the short-range forces that prevent collapse and phase instability. X-ray diffraction studies of forced dehydration of multilamellar lipid-water phases show that the short-range repulsion follows a steep exponential-like decay.[5,51] Hence, the energetics of adhesion for electrically neutral bilayers can be conceptually viewed as approach along a soft van der Waals attraction to a limit determined by the magnitude and decay of the strong repulsion. The free energy potential for assembly of neutral bilayers to stable contact essentially represents the attractive potential at the final separation distance. If the bilayers are unsupported, repulsion may be enhanced by secondary effects due to thermomechanical excitation of bilayer undulations.[52,53] For electrically charged head groups, long-range repulsion follows an exponential decay determined by the characteristic screening distance of the ions in solution as described by Guoy–Chapman theory.[4] At a specific separation z_w, the total free energy per unit area of contact formation is given approximately by[5,53]

$$\tilde{F} = \lambda_{sr}P_{sr}e^{-z_w/\lambda_{sr}} - A_H f(z_1/z_w)/(12\pi z_w^2) + \lambda_{es}P_{es}e^{-z_w/\lambda_{es}} + \tilde{F}_{fl}$$

P_{sr} is the coefficient for the strong short-range repulsion and λ_{sr} is the decay length; A_H is the Hamaker coefficient for the van der Waals attraction, and $f(z_1/z_w)$ is a weak retardation function of the ratio of the bilayer thickness z_1 to the distance between bilayers; P_{es} is the coefficient for the electric double-layer repulsion and λ_{es} is the decay length. The last term in the free energy expression $\tilde{F}_{fl}$ is the free energy excess due to thermally excited mechanical undulations of the bilayers. Equilibrium contact is specified by the stress-free condition at the secondary minimum where the derivative of the free energy potential is equal to zero.

The interactions listed above are given as functions of the same separation distance; however, the actual origin for each interaction is difficult to define because of molecular motion and architecture. The "mass-average" water gap between bilayers seems to be the best functional definition of distance because compositional and colligative properties are based on water content *and* work to remove water from lipid dispersions.[5,13] Compositional and X-ray diffraction studies of lamellar arrays naturally combine to yield the mean water gap with only the assumption of a layered structure.[28] Use of a common distance creates difficulty in the critical evaluation of van der Waals attraction and electric double-layer repulsion when the bilayers are in close proximity ($z_w < 3 \times 10^{-7}$ cm). To circumvent this difficulty, the usual approach is to introduce origins for these interactions which represent the location of head groups and charges relative to the mass-average water interface.

Vesicle–Vesicle Adhesion Tests and Method of Analysis

Adhesion of vesicles is promoted by the attractive potential between surfaces but is opposed by mechanical rigidity of the capsules.[54,55] Because the attraction is weak, frozen bilayer vesicles are usually too rigid to form large contacts by deformation unless there are flat regions that fit together perfectly. On the other hand, bilayers in the L_α (liquid) state easily deform and adhesion spreads to an extent limited by the bilayer tensions as vesicles become pressurized. Mechanical equilibrium translates into the familiar Young equation that relates the free energy potential for membrane assembly to the membrane tension $\bar{\tau}$ and the included angle θ_c between bilayers at the edge of the contact zone

$$\gamma = \bar{\tau}(1 - \cos\theta_c)$$

The adhesion energy (per unit area) γ is defined as minus the free energy potential at the minimum.

Micromechanical experiments to test adhesion follow a procedure similar to that for measurement of membrane mechanical properties.[9,10] Vesicles are first slightly dehydrated to produce large projections into suction pipets. One vesicle is aspirated at high pressure so that the vesicle is pressurized into a rigid sphere. Another vesicle is aspirated into a second pipet at low suction. This vesicle is then maneuvered into proximity of the rigid vesicle surface where adhesion is allowed to occur in discrete (equilibrium) steps regulated by the low suction (Figure 8). Reversibility is verified directly by observation of the decrease in contact area as the suction is increased. With numerical analysis, measurements of extent of coverage of the rigid vesicle (given by the polar height of the adhesion "cap") vs. pipet suction provide the free energy of adhesion per unit area. This approach has been used to quantitate bilayer adhesion in aqueous salt buffers[10] and in salt buffers that contain high concentrations of protein[56] and polymer macromolecules.[9,57]

Free Energy Potentials for Neutral Bilayer Adhesion

Adhesion tests for bilayers composed of neutral PC's (egg PC, DMPC, SOPC) in the L_α state yield comparable values

(50) Lifshitz, E. M. *J. Exp. Theor. Phys. USSR* **1945**, *29*, 94. *Sov. Phys. JETP (Engl. Transl.)* **1956**, *2*, 73.
(51) Lis, L. J.; McAlister, M.; Fuller, N.; Rand, R. P. *Biophys. J.* **1982**, *37*, 657.
(52) Helfrich, W. *Z. Naturforsch. A* **1978**, *33a*, 305.
(53) Evans, E.; Parsegian, V. A. *Proc. Natl. Acad. Sci. U.S.A.* **1986**, *83*, 7132.
(54) Evans, E. *Biophys. J.* **1980**, *31*, 425.
(55) Evans, E.; Parsegian, V. A. *Ann. N.Y. Acad. Sci.* **1983**, *416*, 13.
(56) Evans, E.; Needham, D.; Janzen, J. In *Proteins at Interfaces*, Brash, J., Ed.; American Chemical Society: Washington, DC, in press.
(57) Evans, E.; Needham, D. *Macromolecules*, to be submitted.

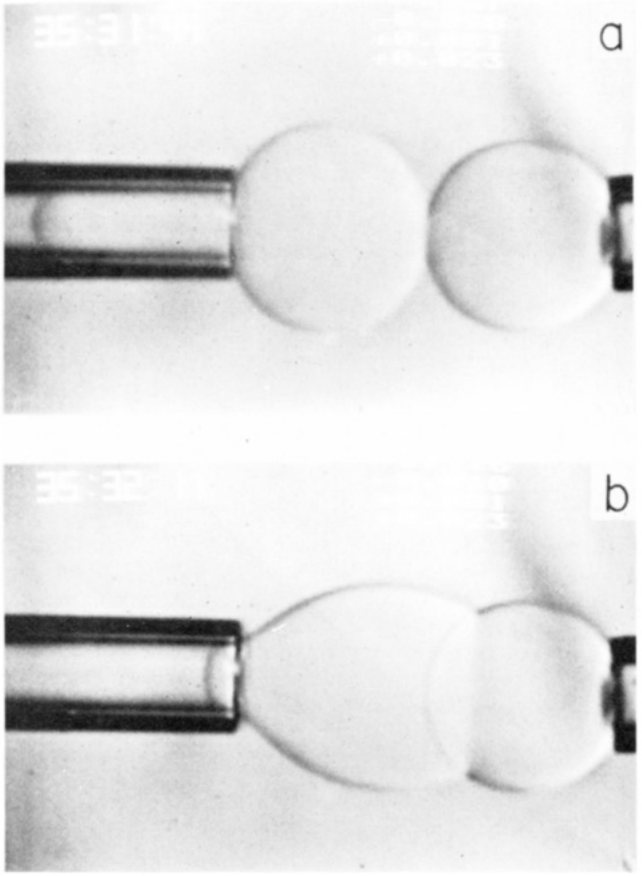

Figure 8. Video micrographs of vesicle–vesicle adhesion test. (a) Vesicles maneuvered into close proximity but not forced to contact. (b) Spontaneous adhesion allowed to progress in discrete steps controlled by suction applied to vesicle on left.

TABLE IV: Mass-Average Water Separation and Parameters for Short-Range Repulsion Derived from X-ray Diffraction Studies[a]

neutral lipid	z_w, $\times 10^{-8}$ cm	P_{sr}, dyn/cm^2	λ_{sr}, $\times 10^{-8}$ cm
SOPC	27	1.0×10^{10}	2.45
POPE	11.5	1.1×10^{12}	0.95
DGDG	13	1.3×10^{11}	1.50

[a] Reference 59.

(0.01–0.015 erg/cm^2) of free energy reduction per unit area of contact.[10,58] Vesicles made from the less-hydrated phospholipid POPE exhibit much stronger adhesion with energies that are an order of magnitude greater (0.12–0.15 erg/cm^2).[3] Even larger free energy potentials (0.22 erg/cm^2) are measured for adhesion with DGDG (sugar-lipid) bilayers.[12,58] Adhesion energies measured for neutral vesicle bilayer attraction are independent of NaCl concentration over the range of 0–0.1 M.[58] At best, these adhesion energies represent three parameters in addition to the equilibrium separation between bilayers: force coefficients (P_{sr}, A_H) for repulsion and attraction and the decay length of the short-range repulsion (λ_{sr}). X-ray diffraction studies of forced dehydration (e.g. by osmotic or mechanical stress) of multilamellar arrays provide the essential measures of separation distance and the interlamellar stress at close range dominated by $P_{sr} \exp(-z_w/\lambda_{sr})$,[5,51,59] given in Table IV.[59] Obviously, larger values of adhesion energy are characteristic of smaller separations at full hydration. However, DGDG and POPE form adhesive contact at similar separations *but* the adhesion energy for DGDG bilayers is nearly twice as strong as that for POPE bilayers. If short-range repulsion is ignored, the equation for van der Waals attraction and values for bilayer separation from Table IV can be used to estimate cumulative Hamaker coefficients for these lipids from the adhesion energies. Coefficients for both phospholipids (PC and PE) are in the range of (6–7) $\times 10^{-14}$ erg whereas the coefficient for DGDG is a factor of 3–4 larger (20×10^{-14} erg). Since the phospholipids and the "sugar"-lipid possess similar acyl chain cores, the conclusion is that the augmented attraction is due to attraction between sugar head groups of DGDG across the water gap.

Because of the significant difference in adhesion energies between lipid bilayers with different classes of head groups (e.g. galactosyl vs. phosphoryl choline or ethanolamine), analysis requires a layered model to reflect specific polarizabilities of head groups, acyl chains, and the interlamellar water phase as given approximately by[60,61]

$$\tilde{F}_A \cong -A_1 f_1/[12\pi(z_w - z_p)^2] - A_2 f_2/[12\pi z_w^2] - A_3 f_3/[12\pi(z_w + z_p)^2]$$

where again z_w is the "mass-average" water separation; $z_p/2$ is the head group projection beyond the mass-average water interface. The retardation functions (f_1, f_2, f_3) depend on the ratios acyl chain thickness:water gap separation and polar head group thickness:water gap separation with values near unity at close range.[60] The Hamaker coefficients (A_1, A_2, A_3) are related to correlations of differences in polarizability between adjacent layers integrated over the electromagnetic spectrum: $A_1 \sim$ (head group–water)^2; $A_2 \sim$ (head group–water)·(acyl chains–head group); $A_3 \sim$ (acyl chains–head group)^2. Simple models of head group geometry indicate projections beyond the mass-average water interface of about 3 Å for the phospholipids and 4–5 Å for DGDG.[12,62,63] For bilayers in close proximity (e.g. POPE and DGDG), head group attraction across the water gap will be the major effect even for small Hamaker coefficients (A_1). At large separations away from equilibrium contact, attraction is characterized by the cumulative coefficient ($A_1 + A_2 + A_3$). Three coefficients for attraction plus geometric properties of the head group allow great freedom in selection of (A_1, A_2, A_3) consistent with measurements of adhesion energy. However, theoretical calculations indicate that the cross coefficient A_2 is very small ($\leq 10^{-15}$ erg) and therefore the second term in the attractive potential can be neglected.[64] Also, these calculations show that the coefficient A_3 for hydrocarbon attraction across the head group region remains essentially constant ($\sim 3 \times 10^{-14}$ erg) for a wide range of head group properties.[60,64] Thus, only the coefficient A_1 is used to correlate the experimental results. For the phospholipids SOPC and POPE, A_1 is estimated to be about 1.2×10^{-14} erg and about 3×10^{-14} erg for the sugar-lipid DGDG. The layered model reduces the cumulative value for the attraction coefficient and leads to reasonable magnitudes for all coefficients ($<10^{-13}$ erg).

If we accept an exponential form for the short-range repulsion, attenuation of the adhesion energy by repulsion is about 10–40% based on the parameters in Table IV; coefficients for attraction must be increased by about 50% to match the measured adhesion energies. If soft repulsive effects exist further out, the energy contribution could be much greater than deduced from $\lambda_{sr} P_{sr} \exp(-z_w/\lambda_{sr})$. For example, softer repulsion is predicted from analysis of thermally excited bending undulations in unsupported bilayers.[52,53] Repulsion is enhanced by the work required to drive heat out of the system as the bilayers are forced together. The enhanced repulsion is calculated to be significant close to and beyond the equilibrium separation distance for bilayers in the L_α phase. For separations less than equilibrium contact, the free energy excess due to bilayer undulations is determined by the short-range repulsion[53]

$$\tilde{F}_{fl} \sim (\pi kT/16)(P_{sr}/B\lambda_{sr})^{1/2} e^{-z_w/2\lambda_{sr}}$$

(58) Evans, E.; Needham, D.; Rand, R. P. *Colloids Surfaces*, to be submitted.
(59) Rand, R. P.; Parsegian, V. A., to be submitted for publication.
(60) Le Neveu, D.; Rand, D. P.; Gingell, D.; Parsegian, V. A. *Biophys. J.* **1977**, *18*, 209.
(61) Ninham, B. W.; Parsegian, V. A. *J. Chem. Phys.* **1970**, *53*, 3398.
(62) Hauser, M.; Pascher, I., Pearson, R. M.; Sundell, S. *Biochim. Biophys. Acta* **1981**, *650*, 21.
(63) McIntosh, T. J.; Simon, S. A. *Biochemistry* **1986**, *25*, 4058.
(64) Parsegian, V. A., private communication.

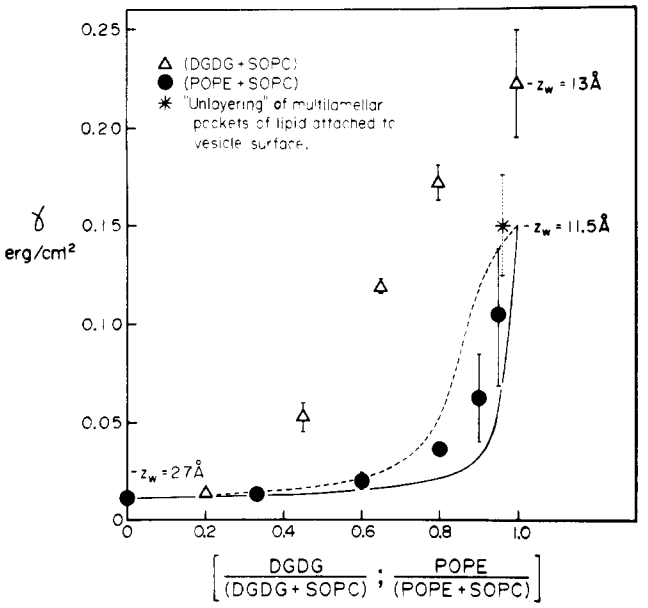

Figure 9. Free energy potentials for adhesion by van der Waals attraction measured with neutral bilayer vesicles vs. composition: either (●) POPE/(POPE + SOPC) or (△) DGDG/(DGDG + SOPC). (Theoretical curves are described in text.)

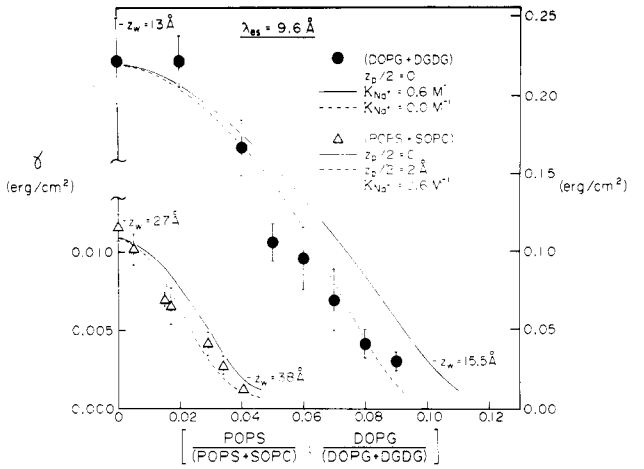

Figure 10. Free energy potentials for adhesion by van der Waals attraction, opposed by electric double-layer repulsion in 0.1 M NaCl, measured with charged vesicles vs. composition: either DOPG/(DOPG + DGDG) or POPS/(POPS + SOPC). Theoretical curves are predictions of classical double-layer theory. Note: ordinate on left side is energy scale for (POPS + SOPC); ordinate on right side is energy scale for (DOPG + DGDG).

where k is Boltzmann's constant. In this range, the primary effect of the added repulsion is to increase the observed decay length λ_{sr} and expand the separation at full hydration. For unsupported SOPC multilayers, analysis shows that the measured 2.45-Å decay would reduce to 2.1 Å if the layers were rigidly fixed to solid substrates. An auxilliary prediction is that the adhesion energy for *immobilized* PC bilayers should be larger than for unsupported PC vesicle membranes. This may account for the stronger adhesion energies measured for PC bilayers adsorbed to rigid mica sheets.[11] At distances well beyond equilibrium separation, the free energy excess from thermomechanical excitations is predicted to follow a weak steric repulsion given by

$$\tilde{F}_{fl} \sim c(\pi kT/16)^2/(Bz_w^2)$$

where $c \cong 5$.[52,53] For neutral bilayers, this weak steric repulsion should overcome the retarded van der Waals attraction at large separations ($>10^{-6}$ cm). However, the repulsive stress is predicted to be so small (<30 dyn/cm^2) that the barrier is insignificant.

"Lipid Mixtures". PC and PE bilayers attract with comparable van der Waals stress but exhibit disparate values of adhesion energy and equilibrium separation because of differences in short-range repulsion. Mixtures have been studied with the expectation that progressive changes in adhesion energy should yield the distance dependence of the attraction as the range of the repulsion is reduced (Figure 9).[3,58] The nonlinear behavior indicates that separation between bilayers changes little with PE content until large amounts of PE are present then the separation is greatly reduced (verified by X-ray diffraction studies of mixtures with the same lipids).[58,59] The simplest approach is to assume a "mixing" relation for the short-range repulsion given by the mole fraction of each lipid multiplied by the exponential repulsion obtained for each pure component (solid curve in Figure 9). If the repulsion is characterized by a dispersive potential with a *constant* decay parameter (consistent with recent polarization-based theories for hydration forces),[65,66] then a different "recipe" for the short-range repulsion would be required. However, the decay lengths for SOPC and POPE are different (Table IV). One patch-up is to superpose two repulsions: the potential-based interaction with a constant decay length plus a *very* short-range steric force common to both lipids (dashed curve in Figure 9). The potential-based repulsion is calculated from the geometric mean of average potentials for each bilayer[3,66]

$$P_{sr} \sim \bar{\psi}_1\bar{\psi}_2$$

where the average potential for each bilayer is given by potentials intrinsic to each lipid molecule multiplied by molar area fractions

$$\bar{\psi} \equiv \alpha_{PE}\psi_{PE} + (1 - \alpha_{PE})\psi_{PC}$$

A more complicated problem arises when results for mixtures of PC and DGDG are examined (also shown in Figure 9).[58] Obviously, "mixing" relations are required for *both* short-range repulsion and van der Waals attraction.

Electric Double-Layer Repulsion between Charged Bilayers in Salt Solutions

Adhesion energies for mixtures of electrically charged (POPS, DOPG) and neutral (SOPC, DGDG) lipids in 0.1 M NaCl are shown in Figure 10. A few percent of charged lipid overcomes the weak van der Waals attraction. Based on area per lipid molecule derived from X-ray diffraction studies[59] (e.g. A_{SOPC} = 66–68 Å,^{2} A_{DGDG} = 72 Å^2) and one electrical charge per PS or PG, adhesion energies are calculated by inclusion of double-layer repulsion in the analysis described previously for neutral bilayers.[69] The curves shown in Figure 10 illustrate the effect of charge position and ion binding. Conceptually, the results can be viewed as reduction of the adhesion energy at essentially fixed separation—as the charge density is increased—followed by a "disjoining" transition where the bilayers separate to large distances. Here, ideal double-layer theory appears to work well at separations of 1–3 debye lengths (λ_{es} = 9.6 Å in 0.1 M NaCl). Furthermore, the outward displacement of the bilayers (implicit in the "disjoining" transition) is consistent with the combined distance dependence for attraction and double-layer repulsion.

(65) Gruen, D. W. R.; Marcelja, S. *J. Chem. Soc., Faraday Trans. 2* **1983**, *79*, 225.

(66) Cevc, C.; Marsh, D. *Biophys. J.* **1985**, *47*, 21.

(67) Eisenberg, M.; Gresalfi, T.; Riccio, T.; McLaughlin, S. *Biochemistry* **1979**, *18*, 3213.

(68) For chemically asymmetric bilayers, small induced bending moments act to wrinkle the membrane and produce tension in the surface. Also, self-adherence of the membrane due to long-range attractive forces can cause the surface to wrinkle and to be stressed. In these situations, the unsupported vesicle maintains a weakly rigid spherical shape.

(69) Double-layer repulsion is modeled by the full-nonlinear Poisson–Boltzmann equations and Guoy–Chapman theory.[4] For these small charge contents, linearized equations are completely acceptable. Also, Na^+ binding to the (PS + PC) bilayers is well-established and is characterized by an equilibrium constant of 0.6 M^{-1}.[67]

Even though there is great practical benefit from evidence that ideal theories are reasonable approximations at small separations (10–30 Å) where these relations are expected to fail, we should not be lulled into complacency. Why do not we observe major deviations from ideality due to structure of the solvent, finite ion size, correlations, and fluctuations? What is the origin(s) of the short-range repulsion and its decay at large separations? Furthermore, does the exponential form for the close-range repulsion hold at very *close proximity*? The power-law attraction should overwhelm the repulsion to cause a precipitous collapse. Clearly, stiff-steric interactions must exist which are of ultimate importance in lamellar phase instability and bilayer coalescence at extreme dehydration.

Acknowledgment. This work was supported by the Medical Research Council of Canada through Grant MT 7477. E.A.E. is grateful to the Alexander von Humboldt Foundation, Federal Republic of Germany, for a Senior Scientist Award.

Registry No. CHOL, 57-88-5; SOPC, 14942-08-6; DOPE, 10015-88-0; DMPC, 13699-48-4; $LysLeu_{16}Lys$, 108260-43-1; $LysLeu_{24}Lys$, 108260-44-2.

ARTICLES

CH Overtones in Acetophenone and Benzaldehyde: Aryl and Methyl Local Modes

T. M. Abdul Rasheed, K. P. B. Moosad, V. P. N. Nampoori, and K. Sathianandan*

Laser Division, Department of Physics, Cochin University of Science & Technology, Cochin 682 022, India
(Received: October 16, 1986; In Final Form: March 17, 1987)

Vibrational overtone spectra of acetophenone and benzaldehyde in the visible and near-infrared regions are studied by the dual beam thermal lens and the conventional near-infrared absorption techniques. The observed increase in the mechanical frequency of the aryl CH bond from that of benzene is attributed to the decrease in the aryl CH bond length caused by the electron-withdrawing property of the substituents. Overtone spectra also demonstrate that acetophenone contains two types of methyl CH bonds arising from the anisotropic environments created by oxygen lone pair and carbonyl π electrons. The local-mode parameters of the two types of CH bonds are compared with those of acetone and acetaldehyde. The possible factors influencing the methyl CH bonds in acetophenone are discussed.

Introduction

Vibrational overtone spectroscopy of molecules containing X–H bonds (X = C, N, O) has been of renewed interest during the past few years.[1,2] The local-mode model is widely used for the description of overtone spectral features.[3-6] This model, introduced by Henry and Siebrand,[7] treats a molecule as a set of loosely coupled anharmonic oscillators localized on individual X–H bonds. Overtone spectra of X–H bonds have been reported for a wide variety of molecules like aromatics,[4] alkanes,[8] and haloalkanes.[9-12] These results have been successfully used for conformational analyses,[10,13] study of nonequivalent CH groups,[8] and substitution effects.[14-18] Such studies have also been extended to nonequivalent CH oscillators produced by anisotropic environments resulting from the lone pair electrons of oxygen and the π electrons of the carbonyl group.[19-23]

In the present paper, we report the overtone spectra of acetophenone and benzaldehyde in the visible and near-infrared regions obtained by dual beam thermal lens and conventional absorption techniques. The mechanical frequencies of the aryl CH bonds in both the molecules show higher values than the corresponding bond in benzene and is attributed to the electron-withdrawing effect of the two substituents. Acetophenone shows two methyl absorption bands arising from two types of CH bonds created by lone pair trans effects and π electrons of the carbonyl bond. The possible factors influencing the strengths of the two types of methyl CH bonds are discussed.

Experimental Section

High-purity acetophenone (99.9% Sisco Research Laboratories, India) and benzaldehyde (99.5% Glaxo BDH, India) are used for the present investigations. The fifth overtone spectra of aryl CH

(1) Henry, B. R. In *Vibrational Spectra and Structure*; Elsevier: New York, 1981; Vol. 10.
(2) Fang, H. L.; Swofford, R. L. In *Advances in Laser Spectroscopy*; Garetz, B. A., Lombardi, J. R., Eds.; Hayden: Philadelphia, PA, 1982.
(3) Henry, B. R. *Acc. Chem. Res.* **1977**, *10*, 207.
(4) (a) Swofford, R. L.; Long, M. E.; Albrecht, A. C. *J. Chem. Phys.* **1976**, *65*, 79. (b) Patel, C. K. N.; Tam, A. C.; Kerl, R. J. *J. Chem. Phys.* **1979**, *71*, 1470.
(5) Fang, H. L.; Swofford, R. L. *J. Chem. Phys.* **1980**, *72*, 6382.
(6) Fang, H. L.; Swofford, R. L. *J. Che. Phys.* **1980**, *73*, 2607.
(7) Henry, B. R.; Siebrand, W. *J. Chem. Phys.* **1968**, *49*, 4359.
(8) Wong, J. S.; Moore, C. B. *J. Chem. Phys.* **1982**, *77*, 603.
(9) Henry, B. R.; I-Fu-Hung. *Chem. Phys.* **1978**, *29*, 465.
(10) Henry, B. R.; Mohammadi, M. A. *Chem. Phys.* **1981**, *55*, 385.
(11) Mortensen, O. S.; Henry, B. R.; Mohammadi, M. A. *J. Chem. Phys.* **1981**, *75*, 4800.
(12) Rasheed, T. M. A.; Nampoori, V. P. N.; Sathianandan, K. *Chem. Phys.* **1986**, *108*, 349.
(13) Henry, B. R.; Thomson, J. A. *Chem. Phys. Lett.* **1980**, *69*, 275.
(14) Mizugai, Y.; Katayama, M. *J. Am. Chem. Soc.* **1980**, *102*, 6424.
(15) Mizugai, Y.; Katayama, M. *J. Am. Chem. Soc.* **1981**, *103*, 5061.
(16) Nakagaki, R.; Hanazaki, I. *Spectrochim. Acta* **1984**, *40A*, 57.
(17) Gough, K. M.; Henry, B. R. *J. Phys. Chem.* **1983**, *87*, 3804.
(18) Gough, K. M.; Henry, B. R. *J. Phys. Chem.* **1983**, *87*, 3433.
(19) Fang, H. L.; Swofford, R. L. *Appl. Opt.* **1982**, *21*, 55.
(20) Nakagaki, R.; Hanazaki, I. *J. Phys. Chem.* **1982**, *86*, 1501.
(21) Fang, H. L.; Meister, D. M.; Swofford, R. L. *J. Phys. Chem.* **1984**, *88*, 405.
(22) Fang, H. L.; Meister, D. M.; Swofford, R. L. *J. Phys. Chem.* **1984**, *88*, 410.
(23) Findsen, I. A.; Fang, H. L.; Swofford, R. L.; Birge, R. R. *J. Chem. Phys.* **1986**, *84*, 16.

0022-3654/87/2091-4228$01.50/0